

GRANULAR FREE SURFACES

PIERRE A. GREMAUD*

Abstract. We explore the notion of angle of repose for granular materials. As an illustration, we solve free surface problems for centrifuged granular piles. These have recently been considered as an affordable and simple way to experiment with powders and dust in reduced gravity environments such as on the Moon or on Mars.

Key words. free surfaces, friction, mechanics, granular material, differential inclusions, partial differential equations

1. Introduction. Consider the following experiment: slowly pour a couple of pounds of sugar on a table. Through successive avalanches, a conical pile will form. Measure the angle between the pile and the table: this is the *angle of repose*. You will find values between 30° and 40° . Now, repeat the experiment with other *granular materials*: salt, flour, potatoes, . . . The angles will be different. What governs this phenomenon?

This seemingly simple question has a long history, largely due to its connection to soil mechanics in civil and military engineering. To date, the mechanics of granular materials is still only partially understood. This is in part due to the important role played by friction and the challenges attached to its mathematical modeling. As a result, our predictive capabilities are limited; this has an enormous economic impact¹. Several elementary issues related to granular materials are considered below.

2. Granular piles. Can we explain the geometry of our pile of sugar?

2.1. Discrete approach. It is natural to look for an explanation in the way the particles are packed together. Their shape plays a significant role: one does not expect the same behavior from, say, grass seeds and gravel. A simple –and classical– stability criterion can be derived for spherical particles of identical size. Note that the spherical assumption is a lot more consistent with potatoes than it is with granulated sugar; more on that later.

Let us look, then, at a pile of spherical particles of equal diameter. We want to add one more particle to the pile at an arbitrary local minimum of the surface: the new particle will be supported by three adjacent, touching spheres of centers A , B and C , respectively, see Figure 2.1. The local angle of the pile is the angle θ between the plane through the centers of the three supporting particles and the table. The orientation of the three particles is characterized by the angle ϕ . Taking only gravity into account, the new particle of center D is stable if and only its projection P on the floor is within the projection of the ABC triangle. This condition is true for small angles θ . A little bit of geometry shows that it remains true for angles $\theta < \theta(\phi)$ where

$$\theta(\phi) = \arctan\left(\frac{1}{2\sqrt{2}\cos\phi}\right). \quad (2.1)$$

*Department of Mathematics, North Carolina State University, Raleigh, NC 27695-8205, USA and Statistical and Applied Mathematical Sciences Institute (SAMSI), Research Triangle Park, NC 27709-4006, USA (gremaud@ncsu.edu). Partially supported by the National Science Foundation (NSF) through grants DMS-0410561.

¹According to [34, 35], improved attention to friction would save developed countries up to 1.6% of their gross national product. Further, solids-processing plants, common in the chemical and pharmaceutical industries, in mining and construction, in food processing, etc..., operate at a much lower percentage of design capacity than their liquids-processing counterparts [37].

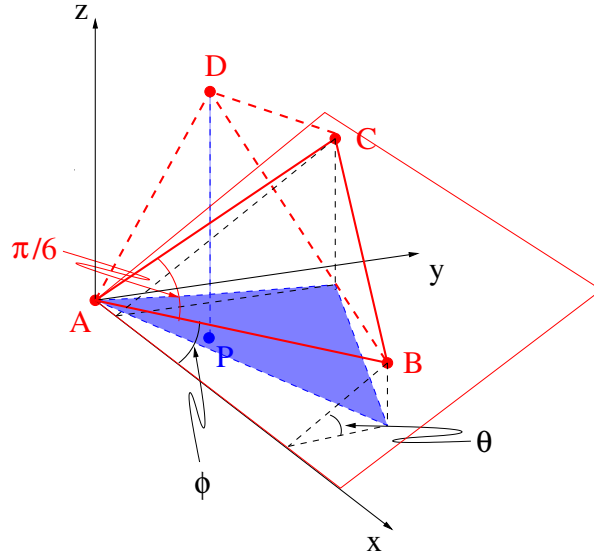


FIG. 2.1. The points A , B and C correspond to the center of three “surface particles”. The plane through those points determine the local slope θ . The stability (or lack thereof) is determined by the location of the projection P of the new particle of center D .

Assuming a uniform random distribution of the orientation of the base ϕ , we take the average to obtain the critical angle θ^*

$$\theta^* = \frac{3}{\pi} \int_0^{\pi/3} \theta(\phi) d\phi \approx 23.8^\circ. \quad (2.2)$$

How close is this to the above table experiment? Not close for sugar: measurements are typically between 28° and 31° [17]. But sugar grains are not spheres. It is barely closer for potatoes which are “better spheres” with a measured angle of repose between 26° and 36° . For spherical glass beads, experimental values of $23.1 \pm 0.4^\circ$ have been reported [22]². While moderately successful for spherical particles, the above geometrical argument is extremely hard to generalize (see [2] for a step in this direction) and seems ill suited for materials with angles of repose that can range from about 20° to over 50° .

2.2. Continuum approach. Coulomb [16] is often credited for being the first to recognize the angle of repose as a material property, see [29] for historical background. This viewpoint regards granular materials as continua. Consider for instance a semi-infinite pile occupying the half space $\{z > 0\}$, see Figure 2.2, left. The equilibrium equations are

$$\nabla \cdot \Sigma = \rho \mathbf{g} \quad \Leftrightarrow \quad \begin{cases} \partial_x \sigma_{xx} + \partial_z \sigma_{xz} = \rho g \sin \theta, \\ \partial_x \sigma_{xz} + \partial_z \sigma_{zz} = \rho g \cos \theta, \end{cases} \quad (2.3)$$

²It is worth noting that granular piles can and do reach angles larger than the angle of repose. Indeed, the latter is measured after landslides have restored stability. Typically, avalanches start at an angle larger than the angle of repose: the angle of maximum stability. This is the angle measured in [22] and is, presumably, the one corresponding to (2.2). For glass beads, the two critical angles differ by about 2° [31].

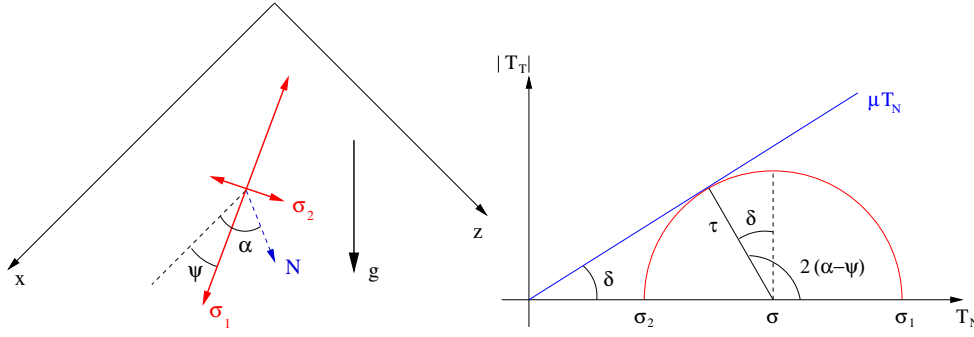


FIG. 2.2. Left: geometry and coordinates of the pile occupying $\{z > 0\}$. The stress stencil is also represented together with its orientation. Right: Mohr circle construction to find the yield condition, see text.

where $\Sigma = \begin{bmatrix} \sigma_{xx} & \sigma_{xz} \\ \sigma_{xz} & \sigma_{zz} \end{bmatrix}$ is the (Cauchy) stress tensor, ρ is the density which is assumed to be constant and \mathbf{g} is the acceleration due to gravity, $g = |\mathbf{g}|$. As is, problem (2.3) is underdetermined: two equations for three scalar unknowns $\sigma_{xx}, \sigma_{xz}, \sigma_{zz}$.

The stress tensor Σ can be rewritten several different ways to facilitate the expression of a constitutive law –the missing relation in (2.3). As a symmetric positive definite matrix, Σ admits an eigenvalue decomposition of the form

$$\Sigma = \begin{bmatrix} \cos \psi & -\sin \psi \\ \sin \psi & \cos \psi \end{bmatrix} \begin{bmatrix} \sigma_1 & 0 \\ 0 & \sigma_2 \end{bmatrix} \begin{bmatrix} \cos \psi & \sin \psi \\ -\sin \psi & \cos \psi \end{bmatrix}$$

where $\sigma_1 \geq \sigma_2 > 0^3$ are the principal stresses (eigenvalues of Σ) and where the angle ψ determines the principal directions. Equivalently, one can also write

$$\Sigma = \sigma \mathbb{I} + \tau U,$$

where $\sigma = \frac{\sigma_1 + \sigma_2}{2}$ is the average stress, $\tau = \frac{\sigma_1 - \sigma_2}{2}$ and $U = \begin{bmatrix} \cos 2\psi & \sin 2\psi \\ \sin 2\psi & -\cos 2\psi \end{bmatrix}$.

Constitutive laws for granular materials reflect the fact that even at rest they can sustain some shearing stress, hence the above piles. Consider a plane of normal $N = \begin{bmatrix} \cos \alpha \\ \sin \alpha \end{bmatrix}$ within the material. The normal stress T_N (a scalar) and tangential stress T_T (a vector) on that surface are respectively

$$T_N = N^t \Sigma N, \quad T_T = \Sigma N - T_N N.$$

The law of sliding friction⁴ postulates

$$|T_T| \leq \mu T_N, \quad (2.4)$$

with deformation taking place if and only if there is equality and where μ is the coefficient of friction of the material. For our piles to stand up, (2.4) has to be

³Granular materials can only sustain compressive stresses.

⁴Relation (2.4), while often attributed to Coulomb, appears to have been first proposed by Amosons in 1699 [3]; see [35] for a nice review of the theory of friction.

satisfied for any α . What kind of constraint does this put on the stress Σ ? To answer this, we first observe

$$T_N = \sigma + \tau \cos 2(\alpha - \psi), \quad |T_T| = |\tau \sin 2(\alpha - \psi)|.$$

Yield is reached for the largest possible value of $|T_T|$ which satisfies (2.4). A geometric representation facilitates answering to the above question: this is the well known Mohr circle construction, see Figure 2.2, right. By inspection of Figure 2.2, right, one sees

$$\frac{\tau}{\sigma} \leq \sin \delta \quad \Leftrightarrow \quad \frac{\sigma_1}{\sigma_2} \leq \frac{1 + \sin \delta}{1 - \sin \delta}, \quad (2.5)$$

where δ is the angle of internal friction which is defined by $\mu = \tan \delta$. This is the missing relation in (2.3) which we can now solve. Solutions to (2.3) in the half-space $\{z > 0\}$ have no x dependency. Adopting a stress free boundary condition on the pile's surface $z = 0$, direct integration of (2.3) leads to

$$\sigma_{xz} = \rho g z \sin \theta, \quad \sigma_{zz} = \rho g z \cos \theta.$$

The last stress component σ_{xx} is at this point a general function of z . Assuming a linear dependency on z , we set

$$\sigma_{xx} = \lambda \rho g z \cos \theta,$$

where λ is a constant to be determined. To find the largest angle θ for which (2.3, 2.5) has a solution, we observe

$$\frac{\tau}{\sigma} = \sqrt{1 + 4 \frac{\tan^2 \theta - \lambda}{(1 + \lambda)^2}},$$

and minimize the right hand side with respect to λ . At the critical value of λ , we have

$$\frac{\tau}{\sigma} = \sin \theta.$$

By comparison with (2.5), it follows that under the above assumption, the steepest angle the pile can take is equal to the angle of internal friction⁵ δ .

3. Spinning it. Assume now that the surface on which the granular material lies is spinning. Think for instance of a bucket of sand spinning around its vertical axis or of a grain spreader. Aside from agricultural applications, this question has important applications in planetary exploration. Indeed, as shown below (see (3.1)), centrifugation reduces the effect of gravitational compressive stresses and as such is an easy way to simulate reduced gravity. For instance, grains settle more slowly on the Moon or on Mars than on Earth due to reduced gravity. As a consequence, features of granular surface which on Earth would be attributed to fluvial flows may in fact just result from reduced gravity [11, 44]. If confirmed, this could provide an explanation of certain channel structures on Mars.

⁵The above argument is not complete in that, among other things, it does not describe the onset of avalanches. Further, it predicts a constant slope of the heap surface, while experiments reveal that the slope may vary slightly. For a growing heap, the slope may become time dependent [24]. Impact of falling particles at the top and interaction with walls at the bottom may also result in departure from constant slope [25]. Models have been proposed to account for those variations [6, 8, 9, 10].

The “spinning” problem for fluids is classical: the top surface of the fluid is a paraboloid of revolution. This is a special case of the present study when no frictional effects are present, i.e., when $\mu = 0$. Note that the source of dissipation in viscous fluids (momentum transfer from collisions) is very different from dissipation in dense granular materials (friction between sliding grains) [41]. The reader can consult [7] for general remarks on the behavior of rotating fluids. A great deal of attention has been given to a slight modification of our case for fluids: the fluid is confined in a *fixed* cylindrical container with only a rotating bottom plate. This configuration gives rise to involved instability phenomena which have been studied both experimentally and theoretically, see for instance [32].

We consider now a rotating frame attached to the container. In this frame, we define cylindrical coordinates (r, φ, z) with the vertical axis z , pointing upward, corresponding to the axis of rotation. The top free boundary \mathcal{S} is expressed as the graph of an unknown function h , i.e.,

$$\mathcal{S} = \{(r, \varphi, z); z = h(r, \varphi)\}.$$

The forces acting on a particle on \mathcal{S} at $(r, \varphi, h(r, \varphi))$ are then

- gravity: $\begin{bmatrix} 0 \\ 0 \\ -mg \end{bmatrix}$, where m is the mass of that particle;
- reaction force: $K = kn$, where k is the magnitude of that force and n is the unit normal vector to \mathcal{S} pointing upward, i.e., $n = \frac{1}{\sqrt{1+(\partial_r h)^2+(\frac{1}{r}\partial_\varphi h)^2}} \begin{bmatrix} -\partial_r h \\ -\frac{1}{r}\partial_\varphi h \\ 1 \end{bmatrix}$;
- friction force: $F = \begin{bmatrix} f_1 \\ f_2 \\ f_3 \end{bmatrix}$; F acts tangentially to \mathcal{S} , i.e.,

$$F \perp n \Leftrightarrow f_3 = f_1 \partial_r h + \frac{1}{r} f_2 \partial_\varphi h$$

and is proportional to k

$$|F| = |\mu K| = \mu |k|.$$

The last relation corresponds to (2.4) for the one particle we are considering. We assume “yield” for now, i.e., the material is at its critical state everywhere (equality instead of inequality). This is not always reasonable and this condition will be relaxed below, see Section 4. The normal acceleration a_n to the surface is given by

$$a_n = g \cos \theta_\ell - \omega^2 r \sin \theta_\ell, \quad (3.1)$$

where θ_ℓ is the local angle of repose, i.e., $\arccos n_z$. The previous relation clearly shows that the centrifugal force mitigates the effects of gravity (at least in the normal direction).

Gathering the information on F yields

$$f_1^2 + f_2^2 + (f_1 \partial_r h + \frac{1}{r} f_2 \partial_\varphi h)^2 = \mu^2 k^2. \quad (3.2)$$

According to Newton’s law, the sum of the above forces equals the product of the mass m by the centrifugal acceleration, i.e.

$$\begin{bmatrix} 0 \\ 0 \\ -mg \end{bmatrix} + \frac{k}{\sqrt{1+(\partial_r h)^2+(\frac{1}{r}\partial_\varphi h)^2}} \begin{bmatrix} -\partial_r h \\ -\frac{1}{r}\partial_\varphi h \\ 1 \end{bmatrix} + \begin{bmatrix} f_1 \\ f_2 \\ f_1 \partial_r h + \frac{1}{r} f_2 \partial_\varphi h \end{bmatrix} = -m\omega^2 r \begin{bmatrix} 1 \\ 0 \\ 0 \end{bmatrix},$$

where ω is the angular velocity. We have neglected the Coriolis force in the previous relation; this assumption is valid provided the speed of the particles measured in the rotating frame stays small with respect to the speed of rotation. This vectorial relation can be rewritten as

$$\begin{bmatrix} \frac{-\partial_r h}{\sqrt{1+(\partial_r h)^2+(\frac{1}{r}\partial_\varphi h)^2}} & 1 & 0 \\ \frac{-\frac{1}{r}\partial_\varphi h}{\sqrt{1+(\partial_r h)^2+(\frac{1}{r}\partial_\varphi h)^2}} & 0 & 1 \\ \frac{1}{\sqrt{1+(\partial_r h)^2+(\frac{1}{r}\partial_\varphi h)^2}} & \partial_r h & \frac{1}{r}\partial_\varphi h \end{bmatrix} \begin{bmatrix} k \\ f_1 \\ f_2 \end{bmatrix} = \begin{bmatrix} -m\omega^2 r \\ 0 \\ mg \end{bmatrix}, \quad (3.3)$$

and used to solve for k , f_1 and f_2 in terms of h and its derivatives. The respective values of k , f_1 and f_2 can then be plugged into (3.2). A little bit of algebra leads to an equation of Hamilton-Jacobi type for h

$$(1 + \mu^2) \left(\omega^2 r \partial_r h + g \right)^2 - (\omega^4 r^2 + g^2) \left(1 + (\partial_r h)^2 + \left(\frac{1}{r} \partial_\varphi h \right)^2 \right) = 0.$$

At this point, we switch to a non-dimensional version of the above equation to better analyze the various effects at play. If L is a characteristic length, for instance the radius of the container or a typical depth, we obtain, keeping the same notation for both h and r

$$(1 + \mu^2) \left(\mathcal{F} r \partial_r h + 1 \right)^2 - (\mathcal{F}^2 r^2 + 1) \left(1 + (\partial_r h)^2 + \left(\frac{1}{r} \partial_\varphi h \right)^2 \right) = 0, \quad (3.4)$$

where all the variables in (3.4) are non-dimensional. The coefficient

$$\mathcal{F} = \frac{\omega^2 L}{g},$$

is a Froude number indicative of the ratio between the centrifugal force and gravity. In the case $\omega = 0$, i.e., $\mathcal{F} = 0$, (no rotation), one finds the Hamilton-Jacobi formulation of a static granular pile as used in [1, 27] (see also the references in Section 6.1), i.e., the Eikonal equation

$$|\nabla h| = \mu. \quad (3.5)$$

4. The axisymmetric case. Assuming no dependence on φ , (3.4) simplifies into the ordinary differential equation

$$(1 + \mu^2)(\mathcal{F} r h'(r) + 1)^2 - (\mathcal{F}^2 r^2 + 1)(1 + h'(r)^2) = 0,$$

where $h'(r)$ denotes the derivative of h with respect to r . This quadratic equation for the slope h' can be readily solved and yields

$$h'(r) = \frac{\mp \mu + \mathcal{F} r}{1 \pm \mu \mathcal{F} r},$$

where the two solutions correspond to the two directions the frictional force F can take. We rewrite the latter equation as

$$h'(r) = \frac{-\lambda + \mathcal{F} r}{1 + \lambda \mathcal{F} r}, \quad (4.1)$$

where λ stands for any number in $[-\mu, \mu]$. More precisely and unlike what is done for instance in [36, 47], the plasticity law is relaxed to allow for noncritical states. Also, as predicted in Section 2, (4.1) reduces to $h'(r) = \mathcal{F}r$ when $\mu = 0$, i.e., for fluids, and a parabolic profile is obtained.

For a fixed value of r , the graph of the right hand side of (4.1) is a hyperbola; only one of the two branches is physically admissible. Indeed, as $\omega \rightarrow 0$, i.e., $\mathcal{F} \rightarrow 0$, the set of admissible slopes should become $[-\mu, \mu]$ (compare with (3.5)). This corresponds to the “right” branch $\lambda > -\frac{1}{\mathcal{F}r}$, see Figure 4.1.

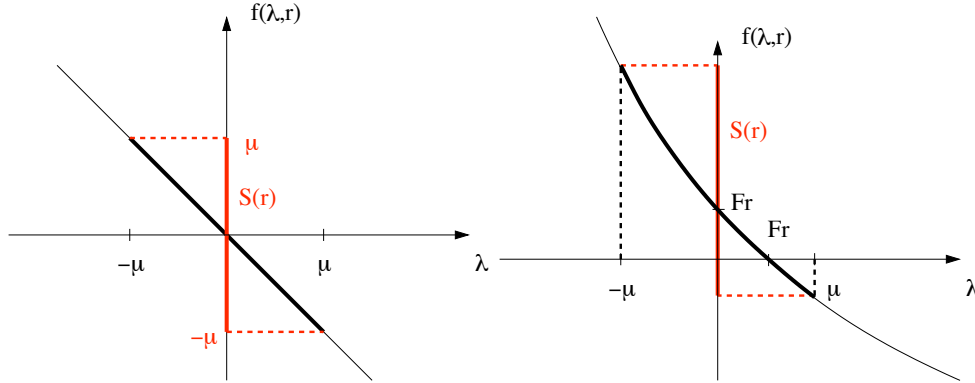


FIG. 4.1. Graph of $f(\lambda, r) = \frac{-\lambda + \mathcal{F}r}{1 + \lambda \mathcal{F}r}$ for a fixed r and for $\mathcal{F} = 0$ (left) and $\mathcal{F} > 0$ (right).

Let $\mathcal{S}(r)$ be the set of admissible slopes at r . A little bit of algebra shows

$$\begin{aligned} \mathcal{S}(r) &= \left\{ \frac{-\lambda + \mathcal{F}r}{1 + \lambda \mathcal{F}r}; \lambda \in \left[\max\{-\mu, -\frac{1}{\mathcal{F}r}\}, \mu \right] \right\} \\ &\equiv [S_{\min}(r), S_{\max}(r)] = \left[\frac{-\mu + \mathcal{F}r}{1 + \mu \mathcal{F}r}, \frac{\mu + \mathcal{F}r}{(1 - \mu \mathcal{F}r)^+} \right], \end{aligned} \quad (4.2)$$

where $(\cdot)^+$ stands for the positive part, i.e., $u^+ = \max(0, u)$. If $\mathcal{F}r > \mu$, then no negative slope is admissible, i.e., $S_{\min} > 0$. Further, if $\mathcal{F}r > \frac{1}{\mu}$ then $(1 - \mu \mathcal{F}r)^+ = 0$ and the interval $\mathcal{S}(r) = [S_{\min}, +\infty)$ becomes semi-infinite. Figure 4.2 illustrates the behavior of \mathcal{S} as a function of r . Equation (4.1) takes the form

$$h'(r) \in \mathcal{S}(r) \in [S_{\min}(r), S_{\max}(r)], \quad (4.3)$$

reflecting the fact that strict static friction is indeterminate. The above problem is a differential inclusion⁶, albeit a quite simple one: the unknown h is absent from the right-hand side. Problem (4.3) has to be completed with a side condition such as fixed height h_0 at one point r_0

$$h(r_0) = h_0, \quad (4.4)$$

⁶Not surprisingly, differential inclusions are harder to analyze than differential equations. Surprisingly maybe, even existence results are harder to come by in general, even though one might naively think that requiring for the derivative to equal a “point” should be harder than requiring it to merely belong to a set. Interested readers can consult two wonderful and engaging papers [13, 15] for more information on this unfortunately very technical area.

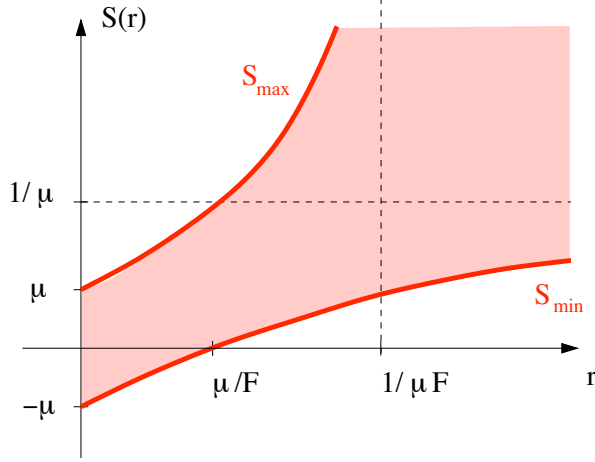


FIG. 4.2. Graph of $r \mapsto \mathcal{S}(r)$. The shaded area corresponds to admissible slopes. The curve \mathcal{S}_{\min} has a horizontal asymptote at $1/\mu$ while the curve \mathcal{S}_{\max} has a vertical asymptote at $1/(\mu\mathcal{F})$.

or given total (non-dimensional) mass m_0

$$2 \int_0^1 h(r) r dr = m_0, \quad (4.5)$$

in a rotating cylindrical container with unit radius. While the existence of solutions is here trivial (pick a curve inside the shaded area of Figure 4.2, integrate it and adjust the integration constant to satisfy either (4.4) or (4.5)), their multiplicity, i.e., non-uniqueness, is just as obvious (pick another curve and proceed as before)⁷.

For the present problem of a vertical bucket spinning on its center vertical axis [36, 47], the observed solution will depend on its “history”. Consider for instance an experiment in which one starts from a horizontal flat surface and ramps up the angular velocity from 0. For $\omega = 0$, i.e., $\mathcal{F} = 0$, the set of admissible slopes is $[-\mu, \mu]$. This corresponds to $\mathcal{S}_{\min} \equiv -\mu$ and $\mathcal{S}_{\max} \equiv \mu$; see again Figure 4.2 for an illustration. The horizontal profile will stay stable provided ω is small enough to render the critical value μ/\mathcal{F} larger than the radius of the cylinder. The slope satisfies

$$h'(r) = \begin{cases} 0 & \text{if } r \leq \frac{\mu}{\mathcal{F}}, \\ \mathcal{S}_{\min}(r) & \text{if } r > \frac{\mu}{\mathcal{F}}. \end{cases} \quad (4.6)$$

Simple integration then yields

$$h(r) = \begin{cases} \bar{h} & \text{if } r \leq \frac{\mu}{\mathcal{F}} \\ \frac{r}{\mu} - \frac{1}{\mathcal{F}} - \frac{1}{\mathcal{F}} \left(1 + \frac{1}{\mu^2}\right) \ln \left(\frac{1 + \mu \mathcal{F} r}{1 + \mu^2} \right) + \bar{h} & \text{if } r > \frac{\mu}{\mathcal{F}}. \end{cases} \quad (4.7)$$

The constant of integration \bar{h} is found from the mass conservation condition (4.5) with an initial constant height h_0 . Figure 4.3 illustrates the behavior of several free

⁷The cases for which h_0 (resp., m_0) in (4.4) (resp. (4.5)) are small enough to lead to a “dry area”, i.e., an area with no material whatsoever, can be treated as well. The “last” grain is located where the frictional and centrifugal forces balance each other. In terms of non-dimensional variables, this corresponds to a radius $r_0 = \frac{\mu_b}{\mathcal{F}}$ where μ_b is the coefficient of friction between the grains and the table. One then looks for h satisfying (4.3) and $h(r_0) = 0$.

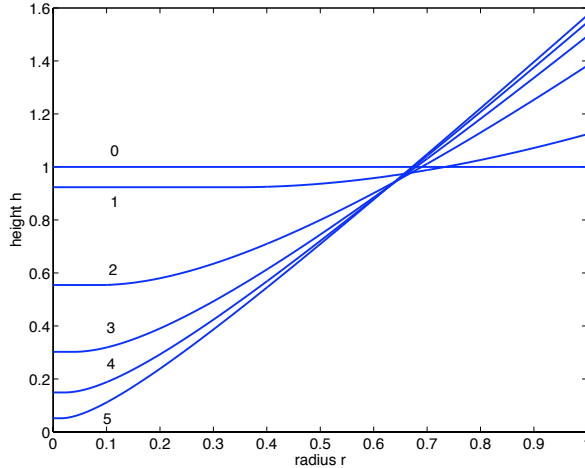


FIG. 4.3. Predicted profiles for Ottawa sand ($\mu = \tan 28^\circ$) in a cylinder of radius 15cm with an initial height of 15cm. The non-dimensionalized height is displayed. Flat initial profile: predicted free surfaces for $\omega = 0, 10, 20, 30, 40, 50$ corresponding respectively to the curves # 0, 1, ..., 5.

surfaces obtained through the above process for various increasing values of the angular velocity ω or, equivalently, increasing values of the Froude number \mathcal{F} . For the larger values of ω , the slope becomes roughly equal to $1/\mu$ as predicted by (4.6). The present approach appears to yield results that agree within measurement error with experimental results, see [36, 47]. Note that if after ramping up the angular velocity ω , one progressively reduces it, the initial profile is clearly *not* recovered. In other words, there are hysteretic effects [48].

Many similar experiments can be considered in conjunction with criteria (4.5) and (4.6). A numerical approach replacing both (4.5) and (4.6) by appropriate quadratures and finite difference formula respectively can easily be considered. For instance, Figure 4.4 illustrates the case of an initial sinusoidal profile.

5. The general case. In the non-axisymmetric case, the problem cannot be reduced to a differential inclusion as was done with (4.6). However, as we did in the previous section, it is possible to find the set of all admissible states by replacing μ by any number $\lambda \in [-\mu, \mu]$, this time in (3.4). In Section 4, for the each value of the radius r , the set of admissible slopes was an interval $\mathcal{S}(r)$ (possibly semi-infinite), see again Figure 4.2. Here, at each r , the set of all admissible gradients

$$\nabla h = [\partial_r h, \frac{1}{r} \partial_\varphi h] \equiv [p, q],$$

is

$$\mathcal{S}(r) = \{(p, q) \in \mathbb{R}^2 \mid \frac{\mathcal{F}^2 r^2 + 1}{(\mathcal{F} r p + 1)^2} (1 + p^2 + q^2) - 1 = \lambda^2 \text{ with } \lambda^2 \in [0, \mu^2]\}. \quad (5.1)$$

A bit of algebra shows that $\mathcal{S}(r)$ is an ellipse if $0 \leq r < \frac{1}{\mu \mathcal{F}}$, a parabola at $r = \frac{1}{\mu \mathcal{F}}$ and a hyperbola for $r > \frac{1}{\mu \mathcal{F}}$. We can now recognize the graph in Figure 4.2 as the $q = 0$ section of the yield surface plotted in Figure 5.1

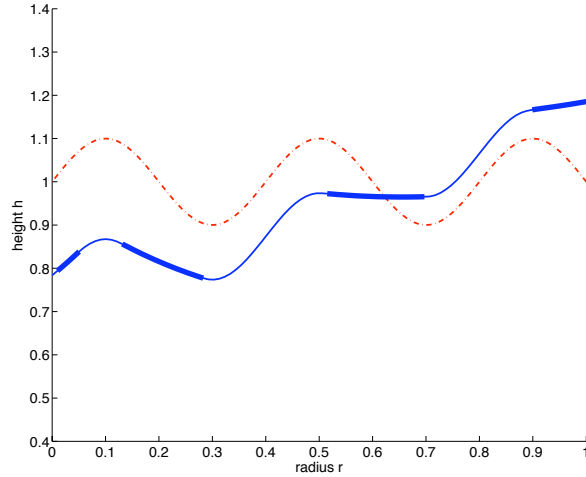


FIG. 4.4. Predicted profiles for a rough material ($\mu = \tan 45^\circ$) such as ground limestone in a cylinder of radius 15cm with an initial height of 15cm. The non-dimensionalized height is displayed. Sinusoidal initial profile (dash dot curve) and final profile (solid curve) for $\omega = 10$. The material is at critical state on the bold portions of the curve.

As was the case in the previous section, the above considerations lead to a local admissibility test for free surfaces. More precisely, at a given point (r, φ)

- test whether $\nabla h(r, \varphi) = [p, q]$ is on or inside the acceptable domain; this can be done easily by computing λ^2 in (5.1); if $\lambda^2 > \mu^2$, then (p, q) is outside of the admissible, otherwise, it is admissible;
- if (p, q) is not admissible, find (p^*, q^*) the closest admissible point to (p, q) ;
- update $h(r, \varphi)$, using the gradient information (p^*, q^*) and the value of h at a “neighboring point” with admissible gradient.

The issue of having to correct a predicted numerical solution by projecting it on a yield surface is classical in computational plasticity, see for instance [45]. For each r , the admissible elasto-plastic domain $\mathcal{S}(r)$ is convex, see again Figure 5.1 and (5.1), which guarantees existence and uniqueness of (p^*, q^*) . In the results presented below, the projection is done numerically.

To implement the above approach, we define a grid on the computational domain $[0, 1] \times [0, 2\pi]$. On a uniform, Cartesian grid, a generic node is $(r_i, \varphi_j) = (i\Delta r, j\Delta\varphi)$, where Δr and $\Delta\varphi$ are the step sizes in r and φ . The partial derivatives p and q in (5.1) are replaced by finite differences, one-sided for the r derivative and centered for the angular derivative. The simplest choices are

$$\begin{aligned} \partial_r h(r_i, \varphi_j) &\approx \frac{h_{i,j} - h_{i-1,j}}{\Delta r} \equiv p_{i,j}, \\ \frac{1}{r_i} \partial_\varphi h(r_i, \varphi_j) &\approx \frac{1}{r_i} \frac{h_{i,j+1} - h_{i,j-1}}{2\Delta\varphi} \equiv q_{i,j}, \end{aligned}$$

where $h_{i,j} \approx h(r_i, \varphi_j)$ but higher order approximations can also be considered. If the gradient at (r_i, φ_j) is not admissible, the height there is updated according to

$$h_{i,j} \leftarrow h_{i-1,j} + \Delta r p_{i,j}^*, \quad (5.2)$$

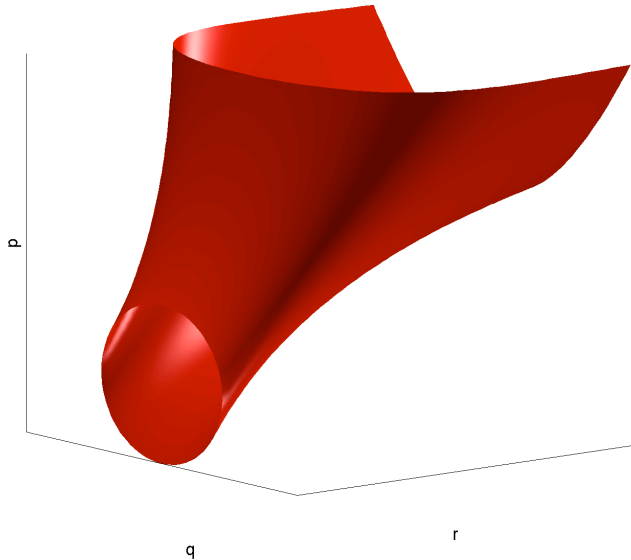


FIG. 5.1. The set of admissible gradients $\nabla h = [p, q]$ is the “inside” of this surface. Figure 4.2 corresponds to the $q = 0$ section of the volume inside this surface.

where $p_{i,j}^*$ is the first component of the projected gradient and the gradient at (r_{i-1}, φ_j) has been deemed admissible. To minimize the propagation of discretization errors, the mesh is traversed one “ $r = \text{constant}$ ” line at a time; in other words, (5.2) is used concurrently for all values of i . The corresponding numerical code has been checked to yield results identical, up to discretization error, to the experiment reported in Figure 4.4, i.e., in the axisymmetric case. Figure 5.2 illustrates the behavior of the free surface in a non-axisymmetric setting.

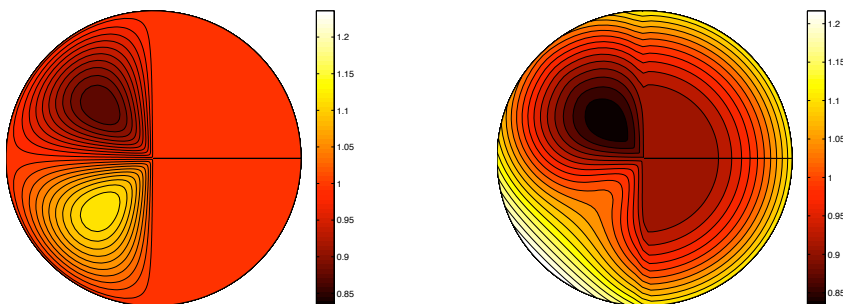


FIG. 5.2. Predicted profile for Ottawa sand ($\mu = \tan 28^\circ$) in a cylinder of radius 15cm with an initial height of 15cm; left: $\omega = 0$, right: $\omega = 10$. The non-dimensional height is displayed.

6. Other granular free surfaces. Many other problems involving granular free surfaces can be found in the literature. We mention a few below and give some corresponding key references without any claim of exhaustivity neither in the choice

of the listed applications nor in the cited contributions.

6.1. Growing sand piles. The problem of growing sand piles has been considered extensively in the literature. Even simple formulations such as [4, 39] lead to surprisingly deep mathematical connections such as the study of the ∞ -Laplacian operator and the Monge-Kantorovich mass transfer theory [5, 18, 19].

An interesting problem is that of growing piles in the presence of obstacles. Assume, to simplify, a horizontal flat area supporting one obstacle (vertical cylinder) of cross-section Ω . For a “one point source” of material at $\mathcal{O} \notin \bar{\Omega}$, determining the height of material of a point \mathcal{P} essentially boils down to finding the shortest distance between \mathcal{O} and \mathcal{P} (exercise!), i.e.

$$d(\mathcal{O}, \mathcal{P}) = \inf \left\{ \int_0^1 \left| \frac{d\gamma}{ds}(s) \right| ds, \gamma \in C^1([0, 1]; \mathbb{R}^2), \gamma(s) \in \mathbb{R}^2 \setminus \Omega \quad \forall s \in [0, 1], \right. \\ \left. \gamma(0) = \mathcal{O}, \gamma(1) = \mathcal{P} \right\}.$$

As done in [1, 27], this can then be related to finding the viscosity solution of simple Eikonal equations with the friction coefficient playing the role of the slowness, see also [21] for a detailed analysis. More involved models of growing sandpiles have been proposed; see for instance [28] for a two layer model and [12] and [20] for respectively mathematical and numerical analysis of it.

Recent experiments reported in [44] have brought to light a wide variety of flow patterns and instability phenomena in centrifuged granular heaps. While the various features observed there are roughly independent of the mass inflow rate, they heavily depend on the kinetic energy of the incoming particles. As is common in granular modeling [41], the present approach does not include energy arguments. The results from [44] are therefore outside the realm of this paper.

6.2. Granular avalanches and landslides. Granular avalanches are more involved than the problems considered above in that motion is not restricted to the upper layers of the material. A large body of literature can be found, starting with the depth-averaged model from [40] to various generalizations of it [23, 30, 33, 38]; see for instance [42, 43] for recent mathematical analysis work.

A related industrial problem is that of slowly rotating, partially filled drums used to mix granular materials. In that case, the axis of rotation is horizontal. Beautiful calculations of the resulting mixing can be found in [26] while the nature of the free surface is discussed in [46].

6.3. Aeolian sand ripples. The formation of sand dunes and ripples is a fascinating example of pattern formation. The grains can move not only through surface creep or reptation as above but also through saltation where they are bouncing off the surface. The seminal work of Bagnold [6] dominated the field for a long time although some of his assumptions have since been disproved (such as the hypothesis that the wavelengths of sand ripples depends on saltation length). A thorough review of existing approaches and results (up to 2005) is available in [14].

7. Conclusion. By following a familiar notion (angle of repose) through one non-standard application (centrifuged granular piles), we have discussed several important aspects of continuum mechanics and applied mathematics. The concepts of plasticity, differential inclusions and solution selection appear naturally in the present setting. Determining the shape of a static granular pile around an obstacle using the

Eikonal equation (3.5) is a highly recommended exercise, both with pencil and paper and in an improvised lab. It is a wonderful introduction to non-linear PDEs.

A much harder “exercise” is the derivation of models for granular materials from first principles. While this question is at the crossroad of several of the most active fields of research in applied mathematics such as stochastic analysis, multi-scale and multi-physics modeling, there is still to date no widely accepted model of the sort.

REFERENCES

- [1] S.A. AHMED, R. BUCKINGHAM, P.A. GREMAUD, C.D. HAUCK, C.M. KUSTER, M. PRODANOVIC, T.A. ROYAL AND V. SILANTYEV, *Volume Determination for Bulk Materials in Bunkers*, Int. J. Numer. Meth., 61 (2004), pp. 2239–2249.
- [2] R. ALBERT, I. ALBERT, D. HORNBAKER, P. SCHIFFER AND A.L. BARABÁSI, *Maximum angle of stability in wet and dry spherical granular media*, Phys. Rev. E, 56 (1997), pp. R6271–R6274.
- [3] G. AMONTONS, *De la Résistance Causée dans les Machines*, Mem. de l’Académie Royale A, (1699), pp. 275–282.
- [4] G. ARONSSON, *A mathematical model in sand mechanics: presentation and analysis*, SIAM J. Applied Math., 22 (1972), pp. 437–458.
- [5] G. ARONSSON, L.C. EVANS AND Y. WU, *Fast/slow diffusion and growing sandpiles*, J. Diff. Eq., 131 (1996), pp. 304–335.
- [6] R.A. BAGNOLD, *The physics of blown sand and desert dunes*, Methuen, 1941.
- [7] G.K. BATCHELOR, *An Introduction to Fluid Dynamics*, Cambridge University Press, 1967.
- [8] R.P. BEHRINGER, *The dynamics of flowing sand*, Nonlinear Sci. Today, 3 (1993), pp. 1–15.
- [9] J.-P. BOUCHAUD, M.E. CATES, J. RAVI PRAKASH AND S.F. EDWARDS, *Hysteresis and metastability in a continuum sandpile model*, Phys. Rev. Lett., 74 (1995), pp. 1982–1985.
- [10] T. BOUTREUX, E. RAPHAËL AND P.G. DE GENNES, *Surface flows of granular materials: a modified picture for thick avalanches*, Phys. Rev. E, 58 (1998), pp. 4692–4700.
- [11] A. BRUCKS, T. ARNDT, J.M. OTTINO AND R.M. LUEPTOW, *Behavior of flowing granular materials under variable g* , Phys. Rev. E, 75 (2007), pp. 032301-1–032301-4.
- [12] P. CANNARSA AND P. CARDALIAGUET, *Representation of equilibrium solutions to the table problem for growing sandpiles*, J. Eur. Math. Soc., 6 (2004), pp. 435–464.
- [13] A. CELLINA, *A view on differential inclusions*, Rend. Sem. Mat. Univ. Pol. Torino, 63 (2005), pp. 197–209.
- [14] D. COCKS, *Mathematical modelling of dune formation*, University of Oxford, 2005, <http://eprints.maths.ox.ac.uk/764/>
- [15] J. CORTÉS, *A tutorial on solutions, nonsmooth analysis and stability*, IEEE Control Systems Magazine, June, (2008), pp. 36–73.
- [16] C.A. COULOMB, *Essai sur une application des règles de maximis & minimis à quelques problèmes de statique, relatifs à l’architecture*, Mémoires de Mathématique & de Physique, présentés à l’Académie Royale des Sciences par divers Savans, & lûs dans ses Assemblées, 7 (1773), pp. 343–382 (Paris 1776).
- [17] C.A. DAVY, M.D. BOLTON AND N.A. FLECK, *The shearing behavior of a sugar aggregate*, Acta Materialia, 52 (2004), pp. 3587–3601.
- [18] L.C. EVANS, M. FELDMAN AND R.F. GARIEPY, *Fast/slow diffusion and collapsing sandpiles*, J. Diff. Eq., 137 (1997), pp. 166–209.
- [19] L.C. EVANS AND W. GANGBO, *Differential equations methods for the Monge-Kantorovich mass transfer problem*, Mem. Amer. Soc., (137) (1999), # 653.
- [20] M. FALCONE AND S. FINZI VITA, *A finite-difference approximation of a two-layer system for growing sandpiles*, SIAM J. Sci. Comput., 28 (2006), pp. 1120–1132.
- [21] M. FELDMAN, *Growth of a sandpile around an obstacle*, Contemp. Math., 226 (1999), pp. 55–78.
- [22] S.P. FRIEDMAN AND D.A. ROBINSON, *Particle shape characterization using angle of repose measurements for predicting the effective permittivity and electrical conductivity of saturated granular media*, Water Resources Res., 38 (2002), pp. 18-1–18-11.
- [23] J.M.N.T. GRAY AND X. CUI, *Weak, strong and detached oblique shocks in gravity-driven granular free-surface flows*, J. Fluid Mech., 579 (2007), pp. 113–136.
- [24] Y. GRASSELLI AND H.J. HERRMANN, *Shapes of heaps and in silos*, Eur. Phys. J.B, 10 (1999), pp. 673–679.
- [25] Y. GRASSELLI AND H.J. HERRMANN, *Crater formation on a three dimensional granular heap*, Granular Matter, 3 (2001), pp. 201–204.

- [26] J.M.N.T. GRAY, *Granular flow in partially filled slowly rotating drum*, J. Fluid Mech., 441 (2001), pp. 1–29.
- [27] P.A. GREMAUD AND C.M. KUSTER, *Accurately Computing the Shape of Sandpiles*, in Multiscale and Optimization Methods and Applications, Editors: W.W. Hager, S.J. Huang, P.M. Pardalos, O.A. Prokopyev, Nonconvex Optimization and its Applications, vol. 82, Springer, 2006, pp. 305–312
- [28] K.P. HADELER AND C. KUTTLER, *Dynamical models for granular matter*, Granular Matter, 2 (1999), pp. 9–18.
- [29] J. HEYMAN, *Coulomb’s memoir on statics*, Cambridge University Press, 1972.
- [30] R.M. IVERSON AND R.P. DENLINGER, *Flow of variably fluidized granular masses across three-dimensional terrain. 1. Coulomb mixture theory.*, J. Geophys. Res. B, 106 (2001), pp. 537–552.
- [31] H.M. JAEGER, C.-H. LIU AND S.R. NAGEL, *Relaxation at the angle of repose*, Phys. Rev. Letters, 62 (1989), pp. 40–43.
- [32] R.N. JANSSON, M.P. HASPANG, K.H. JENSEN, P. HERSEN AND T. BOHR, *Polygons on a rotating fluid surface*, Phys. Rev. Let., 96 (2006), pp. 174502-1–174502-4.
- [33] P. JOP, Y. FORTERRE AND O. POULIQUEN, *A constitutive law for dense granular flows*, Nature, 441 (2006), pp. 727–730.
- [34] H.P. JOST, *Tribology: origin and future*, Wear, 136 (1990), pp. 1–17.
- [35] J. KRIM, *Resource Letter: FMMLS-1: Friction at macroscopic and microscopic length scales*, Am. J. Phys., 70 (2002), pp. 890–897.
- [36] A. MEDINA, *Free surface flow and fracture in granular media*, J. Phys. Soc. Japan, 71 (2002), pp. 1189–1196.
- [37] E.W. MERROW, *A quantitative assessment of R&D requirements for solids processing technology*, Publication R-3216-DOE/PSSP of the Rand Corporation, 1986.
- [38] O. POULIQUEN AND Y. FORTERRE, *Friction law for dense granular flows: application to the motion of a mass down a rough inclined plane*, J. Fluid Mech., 453 (2002), pp. 133–151.
- [39] L. PRIGOZHIN, *Sandpiles and river networks: extended systems with nonlocal interactions*, Phys. Rev. E, 49 (1994), pp. 1161–1167.
- [40] S.B. SAVAGE AND K. HUTTER, *The motion of a finite mass of granular material down a rough incline*, J. Fluid Mech., 199 (1989), pp. 177–215.
- [41] D.G. SCHAEFFER, *Instability in the evolution equations describing incompressible granular flow*, J. Diff. Eq., 66 (1987), pp. 19–50.
- [42] D.G. SCHAEFFER AND R.M. IVERSON, *Steady and intermittent slipping in a model of landslide motion regulated by pore-pressure feedback*, SIAM J. Appl. Math., 69 (2008), pp. 769–786.
- [43] M. SHEARER, J.M.N.T. GRAY AND A.R. THORNTON, *Stable solutions of a scalar conservation law for particle-size segregation in dense granular avalanches*, European J. Appl. Math., 19 (2008), pp. 61–86.
- [44] T. SHINBROT, N.-H. DUONG, M. HETTENBACH AND L. KWAN, *Coexisting static and flowing regions in a centrifuging granular heap*, Granular Matter, 9 (2007), pp. 295–307.
- [45] J.C. SIMO, *Numerical analysis and simulation of plasticity*, in Handbook of Numerical Analysis, Vol. VI, P.G. Ciarlet and J.L. Lions, Eds., Elsevier, 1998, pp. 183–499.
- [46] N. TABERLET, P. RICHARD AND E.J. HINCH, *S shape of a granular pile in a rotating drum*, Phys. Rev. E, 73 (2006), pp. R050301-1–050301-4.
- [47] M.E. VAVREK AND G.W. BAXTER, *Surface shape of a spinning bucket of sand*, Phys. Rev. E, 50 (1994), pp. R3353–3356.
- [48] J. WOJEWODA, A. STEFANSKI, M. WIERCIGROCH AND T. KAPITANIAK, *Hysteretic effects of dry friction: modelling and experimental studies*, Phil. Trans. R. Soc. A, 366 (2008), pp. 747–765.